water

MDPI

Article

Buckling and Ultimate Bearing Capacity of Steel Pipes Jacked in Hard Rocks: A Case Study of a Water Pipeline Project in Zhongshan

Rusen Zhao [1], Zhidong Chen [1], Dinghua Feng [1], Qiping Liu [1], Peiwen Wen [1] and Hongwei Yang [2,3,4,*]

[1] Guangdong No.3 Water Conservancy and Hydro-Electric Engineering Board, Dongguan 523710, China
[2] School of Civil Engineering, Sun Yat-sen University, Guangzhou 510275, China
[3] Guangdong Research Center for Underground Space Exploitation Technology, Sun Yat-sen University, Guangzhou 510275, China
[4] State Key Laboratory for Tunnel Engineering, Guangzhou 510275, China
* Correspondence: yanghw9@mail.sysu.edu.cn

Abstract: Steel jacking pipes are potentially prone to buckling instability, a phenomenon that has received limited attention in hard rock formations. This study reports on the field monitoring of a water pipeline project in Zhongshan City, where the circumferential and hoop strains of steel pipe segments jacked in hard rocks were recorded. The buckling deformation observed during steel pipe jacking, as well as the critical buckling load, was analyzed with the aid of numerical simulations using finite element software. The initial defect for the post-buckling analysis of the steel pipe was selected as the first-order buckling mode. Field monitoring revealed that the loading conditions experienced by the steel pipe segments during the jacking process are complex, leading to significant deformation. Throughout the monitoring process, axial stress at each measurement point underwent tensile-compressive transitions. Numerical results showed the actual critical buckling load increases with wall thickness at a constant length-to-diameter ratio, which is significant for short pipes. For pipes with the same wall thickness and outer diameter, the actual critical buckling load of long pipes is significantly lower than that of short pipes. Additionally, initial defects were found to significantly reduce the actual critical buckling load of the steel pipe. Furthermore, the actual critical buckling load of long pipes is much lower than their yield load, whereas, for short pipes, the critical buckling load is limited by their yield load. Measures for managing buckling deformation of steel pipes in situ were also reported. The findings on critical buckling load and the countermeasures for managing buckling in situ would be valuable for the design and construction stages of similar projects employing pipe-jacking technology in hard rock formations.

Keywords: pipe jacking; hard rocks; buckling stability; critical buckling load

check for updates

Citation: Zhao, R.; Chen, Z.; Feng, D.; Liu, Q.; Wen, P.; Yang, H. Buckling and Ultimate Bearing Capacity of Steel Pipes Jacked in Hard Rocks: A Case Study of a Water Pipeline Project in Zhongshan. *Water* **2024**, *16*, 3041. https://doi.org/10.3390/w16213041

Academic Editor: Stefano Alvisi

Received: 12 August 2024
Revised: 12 September 2024
Accepted: 20 September 2024
Published: 24 October 2024

Copyright: © 2024 by the authors. Licensee MDPI, Basel, Switzerland. This article is an open access article distributed under the terms and conditions of the Creative Commons Attribution (CC BY) license (https://creativecommons.org/licenses/by/4.0/).

1. Introduction

Pipe jacking, in which thin-walled cylindrical shells are jacked into stratum, has the advantages of less ground disturbance and rapid construction in comparison to traditional trench technology and has been increasingly employed in municipal underground space constructions (e.g., [1–3]). Due to its good self-sealing, high strength to bear internal pressure, and better deformation performance, steel pipe has become a common material for pipe jacking, especially in long-distance water pipeline projects (e.g., [4]). Yet, one of the existing challenges in applying steel pipe jacking technology is that the steel pipes are prone to local or global instability deformation under complex loads encountered during jacking or buckling instability (e.g., [5]).

Most studies on the buckling stability of steel pipes have focused on soil layers. Initially, analysis of buckling stability is based on the elastic buckling theory assuming uniform axial or radial pressure under simplified boundary constraints (e.g., [6–8]). Such

assumption is not in accordance with actual conditions in actual jacking projects in which the pipes are subjected to complex loading conditions (e.g., [5,9–11] types and connection methods. Therefore, the relevant studies on thin-walled cylindrical shells cannot be directly applied to the buckling stability analysis of steel pipes in jacking projects. Therefore, studies on buckling instability have been increasingly focusing on the elasto-plastic behavior of large-diameter steel pipes (e.g., [5,9–14]). For example, Chen et al. [12] simplified the water and soil pressure on steel pipes as loads and used finite element methods to study the buckling stability of steel pipes with initial defects under different loads. Zhen et al. [13] used the finite strip method to study the effects of different elastic foundation parameters and geometric parameters of steel pipes on the axial buckling critical load of steel pipes. They [13] also constructed stability analysis models for steel pipes with different stiffening rib forms, analyzing the effects of longitudinal, circumferential, and orthogonal stiffening ribs on the axial buckling stability of steel pipes under various cross-sectional forms, arrangements, and geometric parameters using finite strip and finite element methods. The buckling response of buried steel pipes under different loading conditions has also been investigated through a pipe soil coupling numerical model [5,9–11]. The above-mentioned studies on the buckling stability of steel pipes jacked are in soil layers. Due to the significant differences in loading conditions between hard rock and soil layers, common theories used in soil layers, such as the soil arching theory, are not applicable. Therefore, further research on the buckling stability of long-distance steel pipes in hard rock formations is necessary.

This study reports on the field monitoring of a water pipeline project in Zhongshan City, where the circumferential and hoop strains of steel pipes jacked in hard rocks were recorded. The buckling deformation of steel pipes observed during steel pipe jacking has been analyzed with the aid of numerical simulations. Measures for managing buckling deformation of steel pipes in situ have also been reported.

2. A Water Pipeline Project in Zhongshan

2.1. Project Overview

2.1.1. Geological Conditions

The water pipeline project took place in the suburban area of Zhongshan City, which is located on the mountain Tielushan. The main peak of Tielushan has an elevation of 474 m. During the pipe jacking process, the minimum overburden thickness is only 3 m, while the maximum overburden thickness reaches 286 m. On the west side, in the Shenwan section, the pipe jacking traverses sandy clay, granite, and tuff layers. On the east side, in the Tanzhou section, the pipe jacking primarily encounters sandstone and tuff layers. Additionally, the tuff formations exhibit developed fracture zones and contain a significant amount of fissure water. The overall geological conditions of the pipe jacking path are illustrated in Figure 1. In this study, we focus on the Tanzhou section, in which the majority of the stratum encountered during the jacking process is sandstone and tuff formations (Figure 1b).

The rock in the Tanzhou section consists of tuff and sandstone, with the rock mass classified as intact to moderately intact. The sandstone is slightly to moderately weathered. It is brownish-yellow, bluish-gray, and dark bluish-gray. Core samples are columnar and blocky. Twenty-four rock samples have been tested for uniaxial compression with an average natural compressive strength of 65.1 MPa, a maximum of 144 MPa, and a minimum of 20.5 MPa.

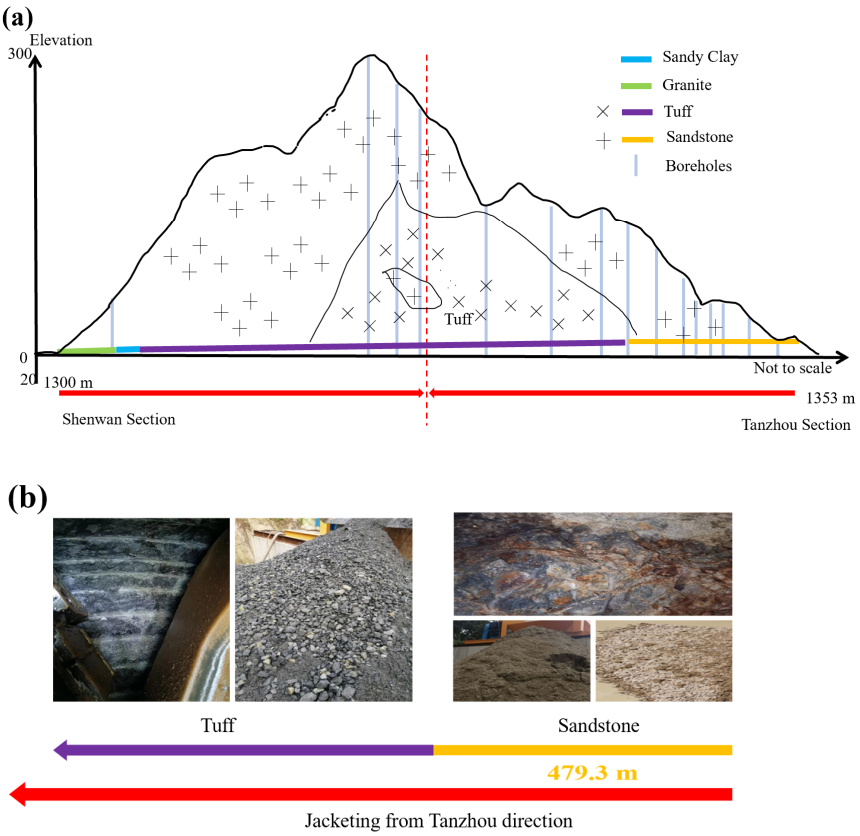


Figure 1. (**a**) Stratum distribution during pipe jacking and (**b**) Rocks encountered in the Tanzhou section.

2.1.2. The Tunnel Boring Machine and Steel Pipes

Based on the characteristics of the rock strata (self-stabilizing excavation face and permeability coefficient greater than 10^{-7} m/s) and the requirements of pipe jacking (such as secondary crushing capability and convenient cutter replacement), slurry balance tunnel boring machines equipped with disk cutters for rock-breaking are chosen in rock pipe jacking projects. In the Tanzhou Section, the HRC 1500 rock tunneling machine, produced by Tangxing Equipment, is chosen. It has an outer body diameter of 1.82 m and a cutterhead cutting diameter of 1.88 m, powered by six hydraulic jacks. Front views of the tunneling machine heads are shown in Figure 2.



Figure 2. Front view of the head of a rock drilling machine.

In this project, Q235 steel pipes are used for the pipe jacking. Each pipe segment is 9 m long, with an outer diameter of 1.8 m and a wall thickness of 22 mm (Figure 3). The

segments are constructed by welding three 3-m-long steel pipes together, with heat-affected zones reserved at both ends of each segment.

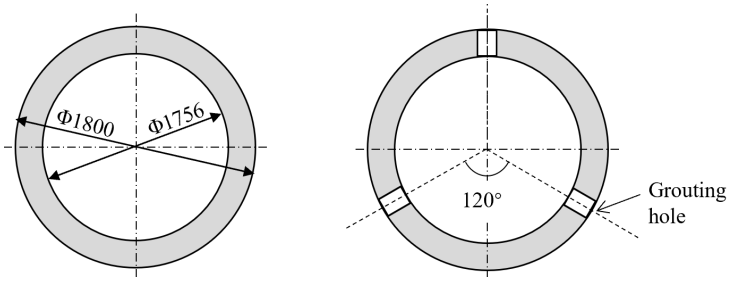


Figure 3. Cross-section of steel pipes and arrangement of grouting holes. (shaded area indicates contact area).

2.2. Field Monitoring of Mechanical Response of Steel Pipes

To understand the stress conditions of the steel pipe sections in the long-distance hard rock pipe jacking project, strain monitoring was conducted during the mid-to-late stages of the east Tanzhou section. Monitoring sections were set up at the 80th and 90th pipe segments, S1 and S2, respectively. The S1 section is located 801.6 m behind the machine head, while the S2 section is 893.3 m behind the machine head (Figure 4).

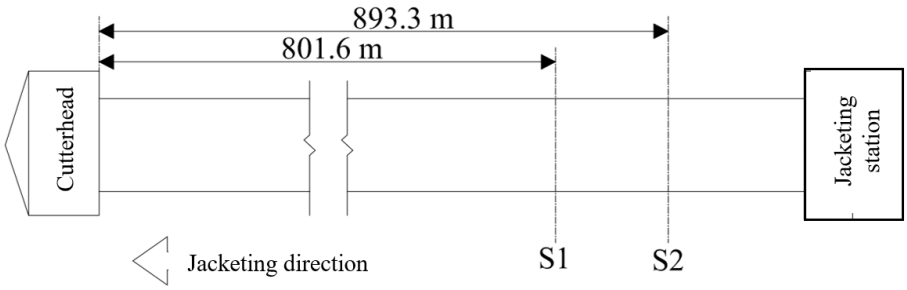


Figure 4. Layout of monitoring sections.

The strain monitoring of the pipe section employs the VS-100B vibrating wire surface strain gauge (Figure 5). This strain gauge is characterized by its simple structure, stable measurements, and the capability to measure the temperature at the embedding point. The measured strain values can be accurately corrected. The gauge has a measurement range of −1500 to 1500 με, operates within a temperature range of −20 to 60 °C, and has a minimum accuracy of 1 με.

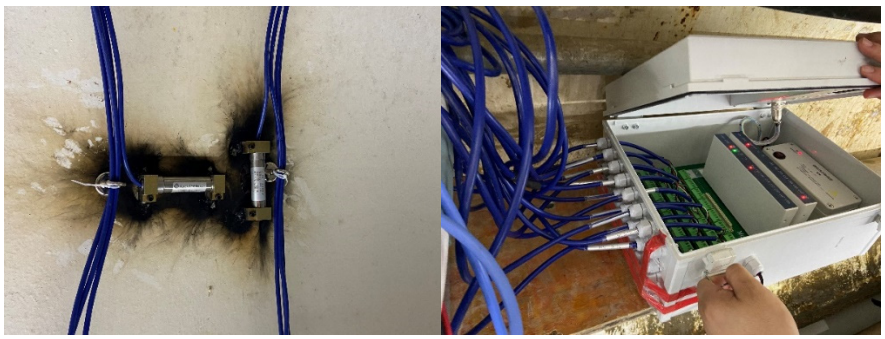


Figure 5. Strain Gauge (**on the left**) and Auto-Harvesting Instrument (**on the right**) Arrangement.

Each monitoring section was equipped with seven measurement points, positioned on the inner wall of the pipe segment at the lower left side, left side, upper left side, top side, upper right side, right side, and lower right side, labeled clockwise from 1 to 7. Due to the

long-distance jacking, the seals in the intermediate sections were partially damaged, causing significant seepage of fissure water to the bottom of the pipes. For welding safety reasons, no strain gauges were installed at the bottom of the pipe sections. At each measurement point, one circumferential strain gauge and one axial strain gauge were installed vertically, distinguished by H and Z, respectively, as illustrated in Figure 6.

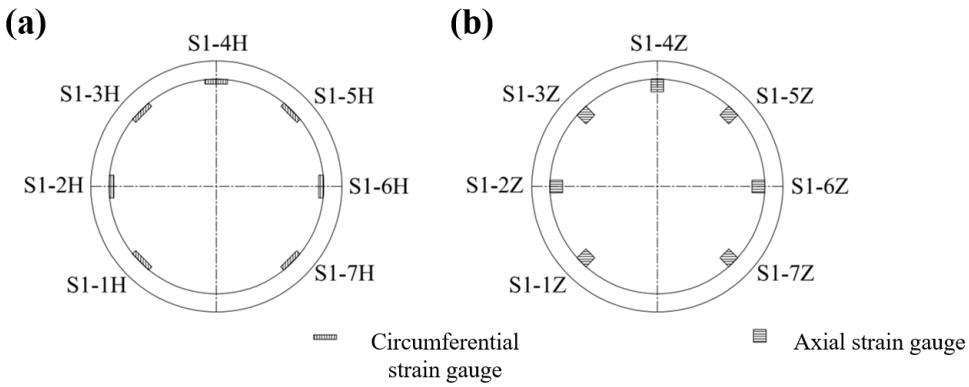


Figure 6. Layout of cross-section measurement points for the (**a**) circumferential strain gauge and (**b**) axial strain gauge.

During the pipe jacking process, the MCU automatic data acquisition instrument collected and stored data from each measurement point at a frequency of once every 10 min. By the time the cumulative jacking distance reached 1392 m, up to 6344 data sets were collected from each measurement point. The axial strain gauge at the lower left side (point 1) was damaged at 1352 m, with a total of 4497 data sets collected. The axial strain gauge at the lower right side (point 7) was damaged at 1364 m, with a total of 5055 data sets collected. Due to engineering safety management issues and power supply reasons, continuous data collection was only allowed after 1279 m of cumulative pipe jacking progress. At this point, the S1 monitoring section had entered the tuff layer, while the S2 section remained in the sandstone layer based on the designed trajectory and rock layer distribution. Data from the S2 section was selected to understand whether the surrounding rock type affects the stress characteristics of the pipeline.

2.3. Results of Mechanical Responses of Steel Pipes

In this project, Q235 steel pipes were used for jacking, with a yield strength of 235 MPa, corresponding to a yield strain range of −1119 to 1119 με. As will be shown later from the monitored axial and circumferential strains of the pipe sections, the steel pipes remained in the elastic deformation stage throughout the jacking process. Therefore, considering the steel pipe as a thin-walled cylindrical structure, the circumferential and axial stresses of the pipe section have been calculated according to the generalized Hooke's law.

2.3.1. Circumferential Mechanical Responses

The variation curves of circumferential strain at different measurement points along the S2 monitoring section with jacking distance are shown in Figure 7. The circumferential stress trends at these points also align with the strain trends. Due to the failure of the axial strain gauges at the lower left (S2-1H) and lower right (S2-7H) points during the late stage III, the subsequent axial strain values at these points could not be measured. Consequently, the circumferential stress values after 1352 m for S2-1H and after 1364 m for S2-7H cannot be calculated. To facilitate description of the curves, the entire monitoring segment is divided into four stages based on the changes in the curves: Stage I (1279 m to 1321 m), Stage II (1321 m to 1350 m), Stage III (1350 m to 1373 m), and Stage IV (1373 m to 1392 m).

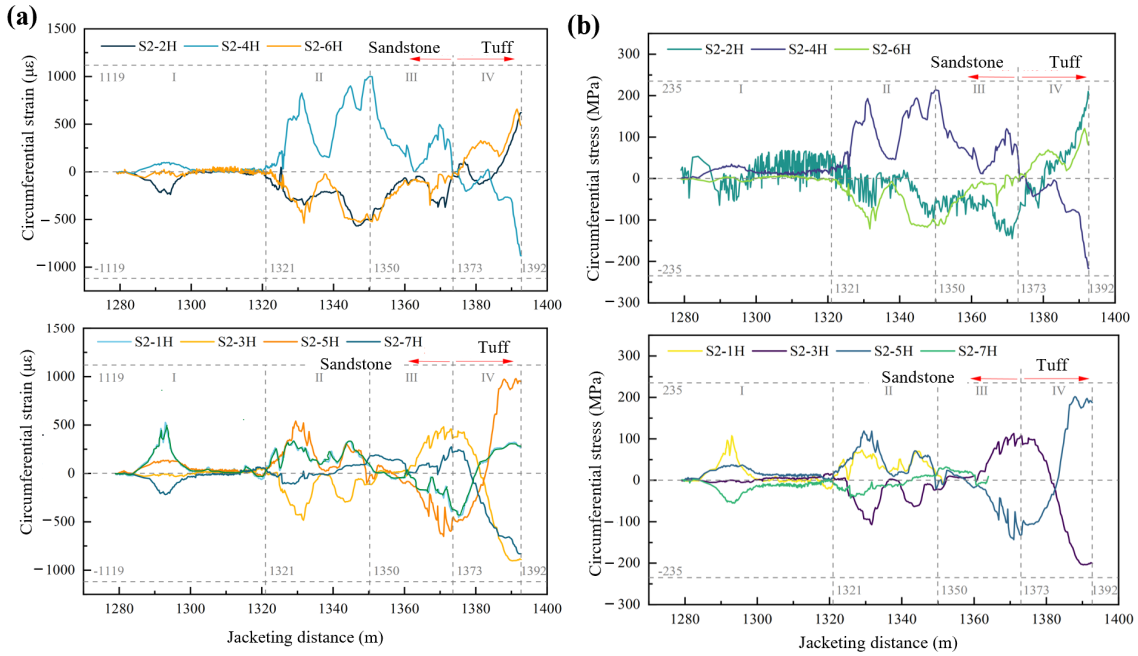


Figure 7. (**a**) Circumferential strain gauge value and (**b**) circumferential stress with jacking distance.

In Stages I and II, the circumferential strain at each measurement point in the monitoring section remains relatively stable. The upper measurement point S2-4H, the lower left point S2-1H, and the upper right point S2-5H all exhibit tensile strain, while the left point S2-2H, right point S2-6H, upper left point S2-3H, and lower right point S2-7H all exhibit compressive strain. The strain magnitudes and variation trends on the left and right sides are generally consistent. The difference in Stage III compared to the previous two stages is that the circumferential strain at the lower left point S2-1H and upper right point S2-5H changes from tensile to compressive, while the strain at the upper left point S2-3H and lower right point S2-7H changes from compressive to tensile. During these three stages, the monitoring section shows an overall circumferential strain pattern of tensile strain at the top and bottom and compressive strain on the sides. It is speculated that the pipe segment is in contact with the surrounding rock due to buoyancy from the slurry.

Additionally, at jacking distances of 1330 m, 1338 m, 1350 m, and 1360 m, changes in strain trends were observed. Considering the tunneling construction status, it was found that at these distances, the project stopped for at least half a day to replace some cutters. During long-distance pipe jacking, lubricating slurry is injected around the pipe segment to reduce friction. Prolonged stoppages lead to significant slurry loss through rock fractures, causing the surrounding rock to undergo convergent deformation to reach a new stress balance. When jacking resumes and slurry is reinjected, the stress state around the pipe changes again, leading to shifts in strain trends at each measurement point.

When jacking reaches Stage IV, strain at all measurement points transitions from tensile to compressive or vice versa. The monitoring section transitions from sandstone to tuff when the jacking distance reaches 1373 m. The change in surrounding rock type directly alters the stress state around the pipe, causing strain at each measurement point to reverse. At this stage, the overall strain pattern in the monitoring section is compressive at the top and bottom and tensile on the sides. As shown in the cross-sectional view of the annular strain state at different stages (Figure 8), with the increasing jacking distance, the monitoring section of the pipe segment tends to deflect towards the upper right. It is speculated that rock debris continuously accumulates at the lower left side of the pipe and, together with the slurry, raises the pipe segment. Additionally, the correction at the machine head in the earlier stage also contributes to the contact between the upper right side of the pipe segment and the surrounding rock.

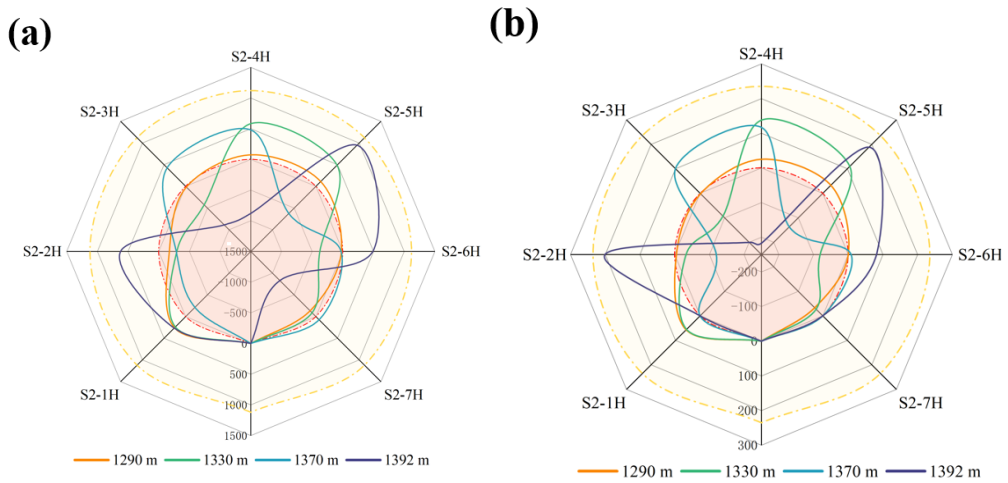


Figure 8. Cross-sectional view of the (**a**) annular strain gauge value and (**b**) stress state at different stages of the jacking process.

2.3.2. Axial Mechanical Response of the Pipe Segment

The axial strain and stress at various measurement points along the S2 monitoring section with jacking distance are shown in Figure 9. Again, for ease of description, the entire monitoring section is divided into four stages based on the curve changes: Stage I (1279 m~1321 m), Stage II (1321 m~1350 m), Stage III (1350 m~1373 m), and Stage IV (1373 m~1392 m).

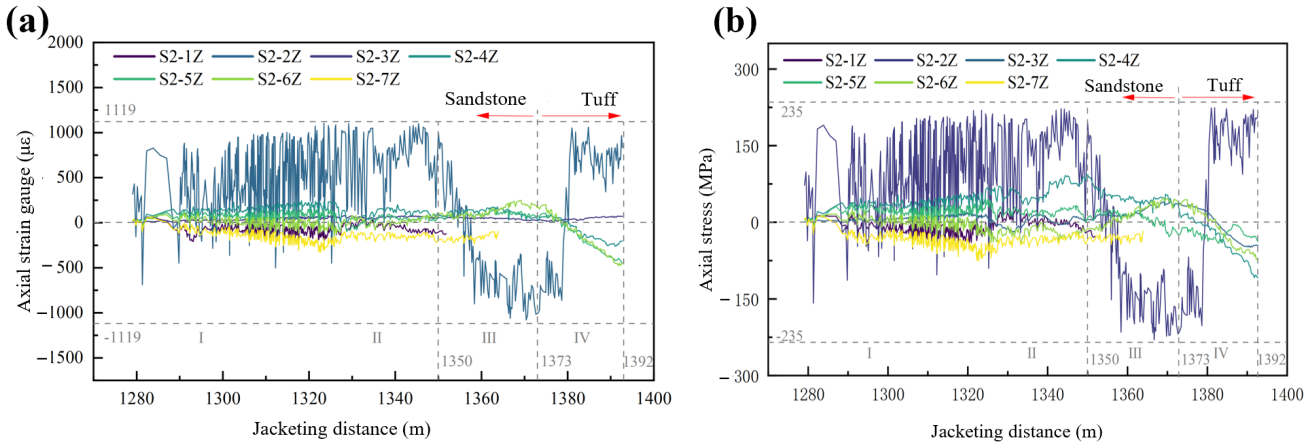


Figure 9. (**a**) Axial strain gauge value and (**b**) axial stress along jacking distance.

During Stages I and II, the absence of debris around the pipe and the complete slurry jack encasing the pipe segment result in stable axial stress and strain values at the monitoring section. The axial strain at the left point S2-2Z, upper left point S2-3Z, upper point S2-4Z, and upper right point S2-5Z is tensile, while the lower left point S2-1Z, right point S2-6Z, and lower right point S2-7Z exhibit compressive strain. The overall axial strain state of the pipe segment in the monitoring section is characterized by compressive strain at the lower right side and tensile strain at the upper left side, with the left point S2-2Z showing significantly higher tensile strain than other points, indicating a rightward deflection tendency of the pipe segment.

In Stage III, the axial strain gauges at the lower left (S2-1Z) and lower right (S2-7Z) points fail, preventing subsequent strain data collection. The left point S2-2Z transitions from tensile to compressive strain, while the right point S2-6Z transitions from compressive to tensile strain. The overall axial strain state of the pipe segment in this stage shows compressive strain at the lower left side and tensile strain at the upper right side, with

the left point S2-2Z displaying significantly higher compressive strain than other points, indicating a leftward deflection tendency of the pipe segment. This strain state change may be attributed to the lag effect of the leftward correction of the machine head during rock pipe jacking on the subsequent pipe segment orientation.

In Stage IV, the left point S2-2Z transitions from compressive back to tensile strain, while the upper point S2-4Z, upper right point S2-5Z, and right point S2-6Z transition from tensile to compressive strain. The overall axial strain state of the pipe segment in this stage shows compressive strain at the upper right side and tensile strain at the upper left side, with the left point S2-2Z displaying significantly higher tensile strain than other points, indicating a rightward deflection tendency of the pipe segment.

These observations illustrate the dynamic axial mechanical response of the pipe segment during the jacking process, influenced by operational conditions and changes in the surrounding rock properties. The transition from Stage III to Stage IV involves a significant change in the surrounding rock properties, which may directly cause local deflection of the pipe segment. The left point S2-2Z transitions from compressive back to tensile stress, while the upper left point S2-3Z, upper point S2-4Z, upper right point S2-5Z, and right point S2-6Z transition from tensile to compressive stress. Notably, although Poisson's effect is present in Stage IV, the circumferential compressive strain at the upper left point S2-3Z significantly exceeds the axial tensile strain, resulting in a predominant circumferential load effect and a compressive axial stress state. The upper right point S2-5Z and right point S2-6Z experience similar levels of circumferential tensile and axial compressive strain, leading to a predominant axial load effect and a compressive axial stress state.

Throughout the entire monitoring stage, all the measured values are always within the nominal yield strength of 235 MPa (Figure 10). The maximum tensile values on the monitoring section are 214 MPa and 223 MPa at circumferential and axial directions, respectively. The compressive stress values on the monitoring section are 217 MPa and 229 MPa at the circumferential and axial directions, respectively.

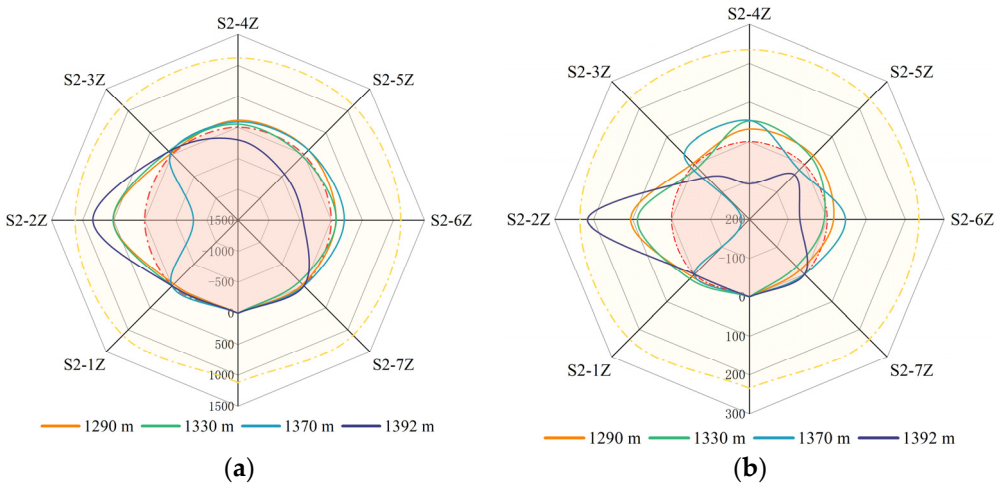


Figure 10. Cross-sectional view of (**a**) axial strain gauge value and (**b**) stress values at different stages.

2.4. Discussions on Monitoring Results and Problems Encountered

The loading conditions experienced by the segment during the jacking process are complex, leading to significant deformation of the pipe segment. Throughout the monitoring process, the axial stress at each measurement point underwent tensile-compressive transitions. This can be attributed to two main factors: 1. Effect of Machine Head Correction: The machine head's correction impacts the subsequent pipeline orientation, causing the pipe segment to experience axial eccentric loads. This eccentric load results in additional stress at the contact points between the locally deflected pipe segment and the surrounding rock, leading to changes in axial stress. 2. Changes in Rock Properties and Slurry Effects: As the cumulative jacking distance increases, the rock properties of the strata traversed

by the monitoring pipe segment change. The pipe segment is influenced by the surrounding slurry and the complex contact state between the pipe and the rock. These factors directly affect the variation in axial stress of the pipe segment. For example, in Stage IV, the left-side measurement point S2-2Z exhibits local tensile stress. This can be explained by the influence of the previous rightward correction of the machine head, causing the left-side measurement point of the pipe segment to mainly experience axial tensile strain. Concurrently, the continuous accumulation of debris beneath the pipe segment, combined with the action of the slurry, lifts the pipe segment. This results in the right upper side of the pipe segment making contact with the surrounding rock while the left side remains in contact with the slurry. Consequently, the left-side measurement point experiences greater circumferential tensile strain than other points. Considering Poisson's effect, this ultimately leads to axial tensile stress on the left side of the pipe segment. This detailed analysis illustrates the dynamic response of the pipe segment's axial stress under varying operational and geological conditions, contributing to the observed deformation patterns during the jacking process.

Despite the complex loading conditions experienced by the segment during the jacking process, causing it to remain in a bent state, the stress on the segment always remained within the yield strength. However, buckling was observed when the cumulative jacking distance reached 663 m. The top of pipe segment 17 exhibited a concave deformation, with the affected area extending 4.7 m and a maximum vertical compression of 28 cm. Inspection through the grouting hole of segment 17 revealed no gravel in the annular gap above the buckling location, ruling out the possibility that the deformation was caused by gravel from a fracture zone or a collapse. It is speculated that the concave deformation might have resulted from local material inconsistencies or defects in segment 17, causing it to buckle under excessive jacking force. The field monitoring data, though, provide direct insights into the mechanical responses of steel pipes during the jacking process and might not explain the observed buckling phenomena. Therefore, a detailed investigation is required for the observed buckling of steel pipes during the jacking process in the Tanzhou section on the east side of Tielushan.

3. Numerical Simulation of Buckling in Steel Pipes Jacked in Hard Rocks

To delve into the observed buckling of steel pipes during the jacking process in the Tanzhou section on the east side of Tielushan, detailed numerical simulations are performed using the ABAQUS finite element software (version 6.14 [15]). Specifically, the ultimate bearing capacity of the steel pipes is simulated and analyzed.

3.1. Numerical Set-Up and Assumptions Used in the Simulations

The numerical simulation analysis of the buckling stability of the steel pipes is based on the following assumptions: 1. The numerical simulation only includes the steel pipe model, disregarding the surrounding rock and pipe-rock interactions; 2. The steel pipe material used in the simulation is the same as that used in the actual project, Q235 steel. The pipeline has been modeled using an elasto-perfectly plastic model by using the following material parameters that include: density ρ = 7850 kg/cm^3, elastic modulus E = 210 GPa, Poisson's ratio μ = 0.3, and yield strength σ_s = 235 MPa; 3. Due to the high diameter-to-thickness ratio of the steel pipes used in the actual jacking project (D/t = 82), shell elements are employed in ABAQUS to simulate the steel pipes; 4. During the long-distance jacking process in hard rock, under grouting conditions, the axial compression on the steel pipe is significantly greater than the confining pressure. Therefore, the subsequent analysis and numerical simulation only consider the effect of axial compression on the buckling stability of the steel pipe; 5. The self-weight of the steel pipe is neglected; 6. During long-distance pipe jacking, varying numbers of intermediate jacking stations are often set up. These stations have high overall stiffness and are unlikely to deform. The steel pipes between the intermediate jacking stations are welded, and the weld seams do not affect the overall stress of the pipeline. Thus, all steel pipes can be considered as a single entity for analysis.

In this simulation, the pipe length is set to the distance between two adjacent intermediate jacking stations, with boundary conditions constraining three directional displacements at one end and circumferential and radial displacements at the other end.

3.2. Buckling Modes of the Steel Pipe

The process of analyzing the buckling stability of steel jacking pipes using ABAQUAS begins with an eigenvalue buckling analysis (buckle analysis step) to determine the potential buckling modes of the steel pipe. The buckle analysis step in ABAQUS is based on linear buckling theory and converts the load into eigenvalues for the solution. Numerical simulations have been performed on pipes longer than the actual segment because the project segments were welded together to form pipelines longer than the segment. Such practice aims to validate the numerical simulations by comparing the simulation results at first-order buckling mode and theoretical values.

Various buckling modes of steel pipes of different lengths under jacking force can be obtained using the buckling analysis step in ABAQUS, as shown in Figure 11. The buckling modes for short pipes exhibit local deformations such as indentations or wave-like patterns; the first-order buckling mode for medium pipes shows overall bending along the pipe length, while the second-order mode displays crests and troughs; the first-order buckling mode for long pipes demonstrates Euler buckling, the second-order mode shows sinusoidal shapes along the pipe length, and the third-order mode displays crests and troughs along the pipe length.

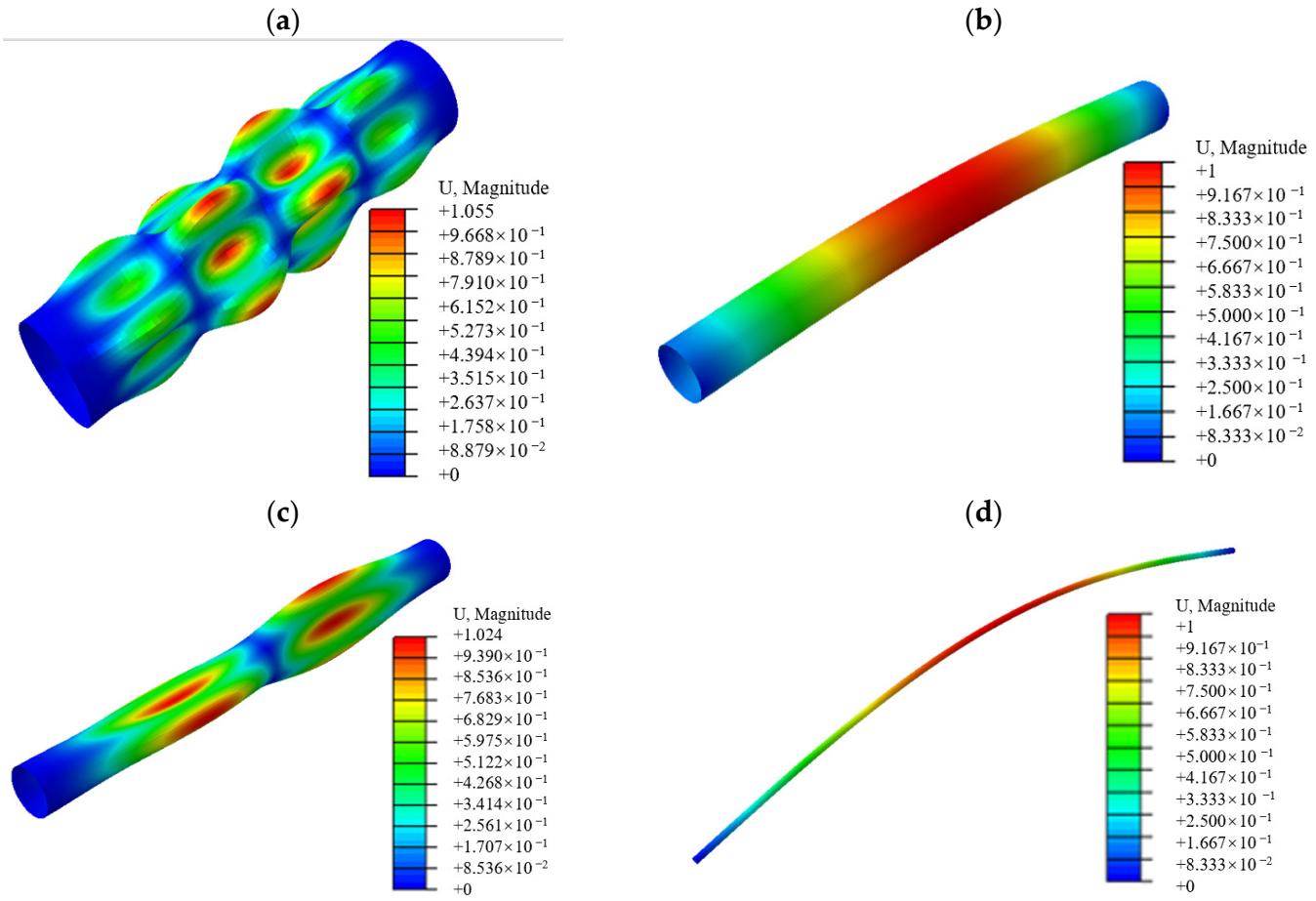


Figure 11. *Cont.*

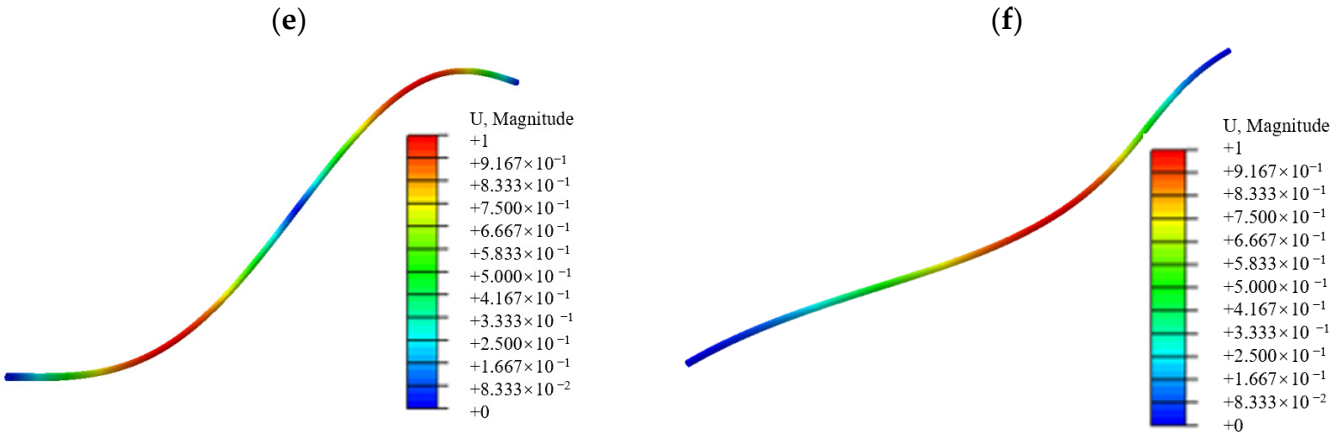


Figure 11. Buckling modes of steel tubes of different lengths. (**a**) First-order buckling mode of an 8 m short pipe; for 20 m medium pipe at (**b**) first-order buckling mode and (**c**) second-order buckling mode; for 207 m long pipe at (**d**) first-order buckling mode (**e**) second-order buckling mode and (**f**) third-order buckling mode.

For steel pipes, the first-order buckling mode is the most critical because it corresponds to the smallest critical buckling load. Therefore, subsequent finite element simulations use the first-order buckling mode as the initial imperfection. The first-order buckling mode represents the ideal elastic buckling mode, typically manifesting as lateral displacement or bending of the steel pipe, yielding a critical buckling load value based on classical elastic theory.

3.3. Validation of Numerical Simulations by Comparing Results with Theoretical Solution

The critical buckling load, P_{cr}, obtained from numerical simulations corresponding to the ith buckling mode that is given by

$$P_{cr} = P_0 + \lambda_i P_\Delta \tag{1}$$

is compared with the theoretical calculations given by Timoshenko and Gere (1965) as

$$P_{cr} = \frac{\pi^2 EI}{(kL)^2} = \frac{\pi^3 E\left[D^4 - (D-2t)^4\right]}{64(kL)^2} \tag{2}$$

where P_0 is the pre-load, λ_i is the eigenvalue of the ith buckling mode, P_Δ is the perturbation load, E is the elastic modulus (GPa), D is the outer diameter of the steel pipe (m), t is the wall thickness of the steel pipe (mm), L is the length of the steel pipe (m), and k is the length coefficient and is taken as 1 for considering the steel pipes to have one end fixed and one end guided.

The critical buckling load obtained from numerical simulations agrees well (with errors within 3%; see Table 1) with theoretical results calculated from Equation (2), which validates the feasibility of using finite element analysis to determine the critical buckling load of steel pipes. The effects of element type, mesh size, and pipe length on critical buckling load have also been investigated for a steel pipe with a diameter of 1.8 m and a wall thickness of 22 mm but with different pipe lengths. For medium and short pipes, using S4R elements with a global mesh size of 0.1 m yields results that are more aligned with theoretical values. For long pipes, using S4R elements with a global mesh size of 0.2 m enhances the accuracy of simulation results compared to theoretical values.

Table 1. Comparison of critical buckling load between numerical simulations and theoretical model with consideration of the effects of mesh type and size on computational accuracy.

Element Type	**S4R**			**S8R**			**Theoretical Value /MN**
Global Mesh Size	**0.1**	**0.2**	**0.5**	**0.1**	**0.2**	**0.5**	
L = 8 m	377.41	392.67	511.21	357.76	359.27	397.54	381.79
L = 50 m	40.38	39.93	36.79	40.40	40.40	40.39	40.26
L = 207 m	2.37	2.34	2.16	2.38	2.38	2.37	2.35

3.4. Ultimate Bearing Capacity of Steel Pipes

In this section, a load-deflection (Riks) analysis is performed to further investigate the buckling problem considering material nonlinearity because real construction pipes inevitably have defects such as minor scratches, dents, or cracks, which can lead to local inhomogeneities and stress concentrations, thus affecting the load-bearing capacity. Particularly, the first-order buckling mode from the buckling analysis step is scaled by a factor to introduce initial imperfections into the pipe for post-buckling analysis using the Riks method. Details about the Riks method can be found in (ABAQUS, 2019).

The ultimate bearing capacity of pipes with different lengths and wall thicknesses is obtained using the Riks method for post-buckling analysis of a steel pipe with initial imperfections and an outer diameter of 1.8 m (Figure 12). The arc length is required in the Riks analysis to measure the progress of the solution. Here, the initial arc length was set to 0.01, the minimum arc length increment to 1×10^{-10}, and the maximum arc length increment to 0.1. Also, in the Riks analysis, a scale factor must be set. From the buckling analysis step, the maximum deformation under the first-order buckling mode is approximately 1.06 m. According to the requirements for pipeline deformation limits in GB 50332-2002 "Code for Design of Structures for Water Supply and Drainage Engineering", the initial imperfection deformation should not exceed 1% of the pipe's outer diameter. Therefore, the scale factor is set to 0.01.

Results for ultimate bearing capacity at different length-to-diameter ratio (L/D; Figure 12) show that with the same L/D, increasing the wall thickness significantly increases the ultimate bearing capacity of the steel pipe. The influence of wall thickness on the ultimate bearing capacity is more pronounced for short pipes compared to long pipes. This is because increasing the wall thickness enhances the bending stiffness and strength of the pipe cross-section, thereby increasing the ultimate bearing capacity. For short pipes, increasing the wall thickness significantly improves their bending resistance, thereby increasing their ultimate bearing capacity. For long pipes, however, the ultimate bearing capacity is influenced by multiple factors, including length, wall thickness, and boundary conditions. While increasing the wall thickness improves the bending stiffness of the cross-section, its impact on the overall long pipe is relatively smaller.

As shown in Figure 12, the ultimate bearing capacity is consistently smaller than the yield loads and critical buckling loads from the theoretical model (Equation (2)), indicating that using critical buckling load or yield load would lead to unconservative estimates of pipe bearing capacity. Specifically, the ultimate bearing capacity of short pipes is close to the yield load but much lower than the theoretical critical buckling load. For long pipes, the ultimate bearing capacity is significantly lower than the yield load and the theoretical critical buckling load. For short pipes, the theoretical critical buckling load is much higher than the yield load, indicating that the pipe begins to yield before buckling, resulting in plastic deformation. The ultimate bearing capacity is, therefore, governed by the yield strength of the pipe, and the actual critical buckling load is limited by the yield load. Thus, in practical construction, the actual critical buckling load of short pipes should be predicted by considering the yield strength to correct the theoretical critical buckling load. Currently, there are semi-empirical formulas, such as the Johnson formula, for predicting the actual critical buckling load of medium and short pipes, which consider both buckling and material yield, thereby improving the reliability of engineering design. Long pipes

undergo elastic buckling as a whole, and the ultimate bearing capacity is the actual critical buckling load.

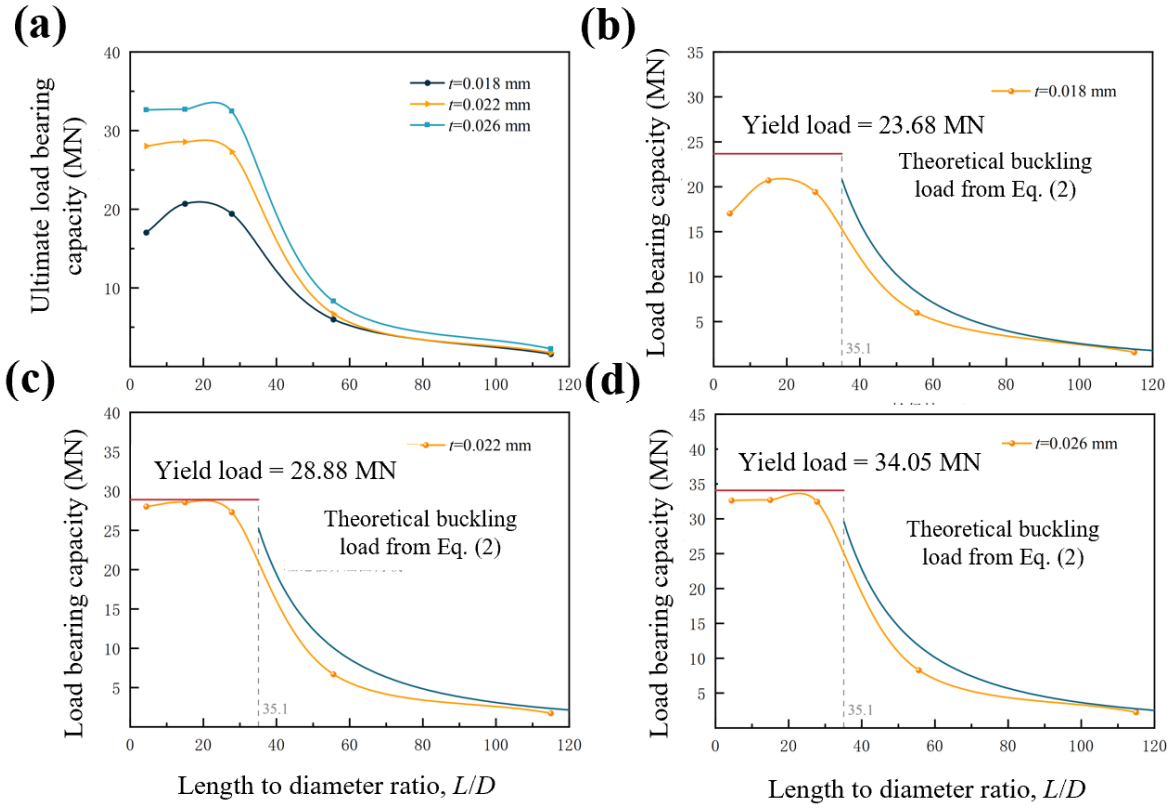


Figure 12. (**a**) Variation of ultimate bearing capacity with length-to-diameter ratio, L/D, and the ultimate bearing capacity at different wall thicknesses (t) for (**b**) t = 0.018 mm, (**c**) t = 0.022 mm, and (**d**) t = 0.026 mm. The blue curve is obtained by using the theoretical model, e.g., Equation (2), which is valid for L/D greater than 35.1.

Moreover, the actual critical buckling load of both short and long pipes is lower than the theoretical critical buckling load, indicating that initial imperfections significantly reduce the critical buckling load of steel pipes. For pipes with the same wall thickness, the ultimate bearing capacity of long pipes is significantly lower than that of short pipes. The ultimate bearing capacity of long pipes decreases with increasing length-to-diameter ratio, while the ultimate bearing capacity of short pipes slightly increases with increasing length-to-diameter ratio. This is because long pipes primarily undergo elastic buckling, with the actual critical buckling load being much lower than the yield load. For short pipes, the actual critical buckling load is limited by the yield load. Increasing the length-to-diameter ratio of long pipes reduces their bending stiffness, thereby decreasing their actual critical buckling load. For short pipes, as the length-to-diameter ratio increases, the boundary conditions may become relatively closer to ideal supports, slightly increasing their actual critical buckling load.

A comprehensive evaluation of the bearing capacity would need to consider the connection/joint between each pipe segment, and such evaluation would require a refined numerical model with increased computational resources and costs. It is foreseen that the joints would reduce the pipe-bearing capacity. Therefore, both the numerical simulations and theoretical calculations might overestimate the bearing capacity.

4. Analysis of Buckling in Steel Pipes Jacked in Hard Rocks

4.1. Pipe Buckling in Tielushan Project

During the hard rock steel pipe jacking construction on the Tanzhou section on the eastern side of Tielushan, buckling was observed on the upper part of pipe segment No. 17 after the cumulative jacking distance reached 663 m. The deformed area was 4.7 m long, with a maximum vertical compression of 28 cm. According to the steel pipe buckling stability analysis from the previous section, pipe segment No. 17 is located between the machine head alignment pipe and relay station No. 1, with the total length of the steel pipes between them being 472 m. At this point, relay station No. 1 provides an axial thrust force of 5.97 MN. This value is significantly smaller than the yield load of the steel pipe, being 28.88 MN. Using ABAQUS finite element software for simulation analysis, the critical buckling load of the steel pipe with initial defects was found to be 0.4 MN, with a maximum critical vertical displacement of 9.77 cm. This indicates that the steel pipe underwent elastic buckling deformation due to excessive jacking force. Through the grouting hole of pipe segment No. 17, it was found that there were no crushed stones in the annular space above the buckling position, ruling out the possibility that the deformation was caused by crushed stone or collapse in the fracture zone. It is suspected that the deformation may have occurred because of local material inconsistencies or defects in pipe segment No. 17, leading to buckling under excessive jacking force. Therefore, the previous analysis highlights the need to increase quality control of the pipe segment, which necessitates consideration of material imperfections in the numerical analysis.

4.2. Measures for Managing Buckling Deformation of Steel Pipes

For steel pipes that have undergone buckling deformation, the first step is to use vertical jacks to restore the buckling deformation area. Following this, a 20 mm thick steel plate is employed as a reinforcing rib to strengthen the steel pipe and enhance its critical buckling load, as illustrated in Figure 13. Additionally, during subsequent jacking processes, it is crucial to strictly control the jacking force. Promptly clearing the annular space of rock debris through opening holes and monitoring the grouting effect is necessary to ensure that the jacking force remains within the critical buckling load of the steel pipe. By implementing these measures, the structural integrity of the steel pipes can be maintained, and the risk of buckling during the jacking process can be significantly minimized.



Figure 13. Steel pipe restoration and reinforcement.

5. Conclusions

This study presents the results of field monitoring of the mechanical responses of steel pipes jacked in hard rock formations. The buckling of steel pipes during jacking in such formations was observed and explained using numerical simulations.

Field monitoring revealed that the loading conditions experienced by the steel pipe segments during the jacking process are complex, leading to significant deformation. Throughout the monitoring process, axial stress at each measurement point underwent

tensile-compressive transitions, influenced by machine head correction and changes in rock properties.

Using a numerical model for steel jacking pipes under axial loading conditions, the effects of different wall thicknesses and pipe lengths on the critical buckling load were studied. The results showed that the actual critical buckling load increases with wall thickness at a constant length-to-diameter ratio. This influence of wall thickness is more significant for short pipes than for long pipes. For pipes with the same wall thickness and outer diameter, the actual critical buckling load of long pipes is significantly lower than that of short pipes. Additionally, the critical buckling load of long pipes decreases with an increase in the length-to-diameter ratio, while for short pipes, it slightly increases with the length-to-diameter ratio.

Numerical simulations considering pipes with initial imperfections showed that these imperfections significantly reduce the actual critical buckling load compared to the theoretical critical buckling load. Furthermore, the actual critical buckling load of long pipes is much lower than their yield load, whereas, for short pipes, the critical buckling load is limited by their yield load.

Author Contributions: Conceptualization, R.Z. methodology, R.Z. and Z.C.; formal analysis, R.Z., D.F. and P.W.; investigation, Z.C., D.F., Q.L. and P.W.; resources, H.Y.; writing—original draft preparation, R.Z. and Z.C.; writing—review and editing, H.Y.; supervision, H.Y.; funding acquisition, H.Y. All authors have read and agreed to the published version of the manuscript.

Funding: This research was funded by Department of Science and Technology of Guandong Province grant number 2021ZT09G087.

Data Availability Statement: The data presented in this study are available on request from the corresponding author.

Acknowledgments: The financial support by Department of Science and Technology of Guandong Province (2021ZT09G087) provide to H.Y are gratefully acknowledged.

Conflicts of Interest: The authors declare no conflicts of interest.

References

1. Ma, B.; Najafi, M. Development and applications of trenchless technology in China. *Tunn. Undergr. Space Technol.* **2008**, *23*, 476–480. [CrossRef]
2. Liu, K.; Xiao, A.; Zhang, P.; Zhou, H.; Chen, Z.; Xu, T.; Ma, B.; Ai, H.; Wang, Q. Study on mechanical re-sponse of steel pipe jacking considering the effect of pipe sticking. *Tunn. Undergr. Space Technol.* **2022**, *127*, 104617. [CrossRef]
3. Feng, X.; Zhang, P.; Chen, X.; Zhang, Y.; Ma, B.; Liu, K.; Xu, T.; Zeng, C. Field mechanical properties of large section concrete pipes during jacking in fractured moderately weathered siltstone. *Tunn. Undergr. Space Technol.* **2023**, *131*, 104818. [CrossRef]
4. Chen, P.; Liu, X.; Deng, Z.; Liang, N.; Du, L.; Du, H.; Huang, Y.; Deng, L.; Yang, G. Study on the pipe friction resistance in long-distance rock pipe jacking engineering. *Undergr. Space* **2023**, *9*, 173–185. [CrossRef]
5. Zhang, J.; Zhang, H.; Zhang, L.; Liang, Z. Buckling Response Analysis of Buried Steel Pipe under Multiple Explosive Loadings. *J. Pipeline Syst. Eng. Pract.* **2020**, *11*, 04020010. [CrossRef]
6. Koiter, W.T. *The Stability of Elastic Equilibrium*; National Aeronautics and Space Administration: Washington, DC, USA, 1970.
7. Simitses, G.J. Buckling and Postbuckling of Imperfect Cylindrical Shells: A Review. *Appl. Mech. Rev.* **1986**, *39*, 1517–1524. [CrossRef]
8. Budiansky, B.; Hutchinson, J.W. A Survey of Some Buckling Problems. *J. Spacecr. Rocket.* **2003**, *40*, 918–923. [CrossRef]
9. Zhang, J.; Liang, Z.; Han, C. Failure Analysis and Numerical Simulation of the Buried Steel Pipeline in Rock Layer Under Strike-Slip Fault. *J. Fail. Anal. Prev.* **2015**, *15*, 853–859. [CrossRef]
10. Zhang, J.; Liang, Z.; Han, C.; Zhang, H. Buckling behaviour analysis of a buried steel pipeline in rock stratum impacted by a rockfall. *Eng. Fail. Anal.* **2015**, *58*, 281–294. [CrossRef]
11. Zhang, J.; Xie, R.; Zheng, T.; Lu, G.; Xu, J.Y. Buckling behavior of buried pipe crossing stratum subsidence area. *Eng. Fail. Anal.* **2022**, *135*, 106130. [CrossRef]
12. Chen, N.; Chen, J.; Xia, X.; Wang, J.; Zhong, J. FEM Analysis on the Buckling of a Long Steel Jacking Pipe. *J. Shanghai Jiao Tong Univ.* **2012**, *46*, 832. (In Chinese)
13. Zhen, L.; Chen, J.-J.; Qiao, P.; Wang, J.-H. Analysis and remedial treatment of a steel pipe-jacking accident in complex underground environment. *Eng. Struct.* **2014**, *59*, 210–219. [CrossRef]

14. Zhen, L.; Qiao, P.; Zhong, J.; Chen, Q.; Chen, J.-J.; Wang, J.-H. Design of steel pipe-jacking based on buckling analysis by finite strip method. *Eng. Struct.* **2017**, *132*, 139–151. [CrossRef]
15. ABAQUS. *ABAQUS/Standard User's Manual, Version 6.14*; Dassault Systèmes Simulia Corp: Providence, RI, USA, 2019.

Disclaimer/Publisher's Note: The statements, opinions and data contained in all publications are solely those of the individual author(s) and contributor(s) and not of MDPI and/or the editor(s). MDPI and/or the editor(s) disclaim responsibility for any injury to people or property resulting from any ideas, methods, instructions or products referred to in the content.